Journal of Alloys and Compounds 492 (2010) 269–276

Contents lists available at ScienceDirect

Journal of Alloys and Compounds

journal homepage: www.elsevier.com/locate/jallcom

# Surface roughness, mechanical properties and bonding structure of silicon carbon nitride films grown by dual ion beam sputtering

Fei Zhou [a,*], Bin Yue [a], Xiaolei Wang [a], Xuemei Wu [b], Lanjian Zhuge [b]

[a] *Nanjing University of Aeronautics and Astronautic, Nanjing, Jiangsu, 210016, China*
[b] *College of Physics, Soochow University, Suzhou, Jiangsu, 215006, China*

ARTICLE INFO

*Article history:*
Received 27 August 2009
Received in revised form 6 November 2009
Accepted 6 November 2009
Available online 13 November 2009

*Keywords:*
Silicon carbon nitride film
Roughness
Hardness
Bonding structure

ABSTRACT

Silicon carbon nitride (SiCN) films were deposited by dual ion beam sputtering (DIBS) of SiC target in mixed $Ar/N_2$ atmosphere at 100 °C. The surface roughness and the mechanical properties of the SiCN films were measured by using non-contact surface profilometer and nano-indenter. The bonding structure for the SiCN films was analyzed using Fourier transform infrared spectroscopy (FTIR), Raman spectroscopy and X-ray photoelectron spectroscopy (XPS), respectively. The influences of assisting ion beam energy and concentration on surface roughness, mechanical properties and bonding structure of the SiCN films were discussed systematically. The results showed that the variations of surface roughness and hardness for the SiCN films with the assisting ion beam energy were in the range of 7–27 nm and 23–29 GPa, respectively. With an increase in the nitrogen ion beam concentration, the film surface roughness first decreased to a minimum value, and then increased, while the hardness first increased to a peak value, and then decreased. When the assisting ion beam energy and concentration were 300 eV and 0.5, the SiCN film possessed the low surface roughness of 11 nm and the highest hardness of 29 GPa, its atoms ratio, C:Si:N:O was about 1:0.42:0.18:0.32. The bonding structure of the SiCN films mainly consisted of Si–C, Si–N, C–N, C=N and C=C bonds and corresponded to a network of the mixed $sp^2/sp^3$ hybridized bonds with the units of $Si(C_4)$, $Si(N_4)$ and $Si(C_{4-n}N_n)$. The film mechanical properties were correlated to the proportion of Si–C, Si–N, C=N and C–N bonds in the SiCN films.

© 2009 Elsevier B.V. All rights reserved.

## 1. Introduction

Due to short bond length, high bond strength and wide band gap, the ternary Si–C–N films possess high hardness [1–3], adjustable friction coefficient [4], high resistance to wear and corrosion [4–8] and play an important role in solar cell, flat panel displays, optical memories [9] as well as Cu diffusion barriers [10]. So far, the silicon carbon nitride (SiCN) films have been synthesized by using different chemical vapor deposition (CVD) methods, such as microwave plasma chemical vapor deposition (MW-CVD) [11,12], electron cyclotron resonance plasma chemical vapor deposition (ECR-CVD) [1,10], hot wire chemical vapor deposition (HWCVD)[13,14], plasma-enhanced chemical vapor deposition (PECVD) [8,15,16], vapor-transport chemical vapor deposition (VT-CVD) [17]. Besides the above various CVD methods, the SiCN films also have been deposited by ion implantation [5,6] and various physical vapor deposition (PVD) methods, such as ion beam sputtering [1,11,18] and magnetron sputtering [2–4,9,19–22].

Actually, whether the SiCN films contained amorphous or crystalline phases would depend on the process conditions. Chen et al. [11] indicated that Si incorporation was crucial for crystal growth with the CVD methods while excessive Si addition in the PVD process induced amorphization of the SiCN films. If the SiCN films were deposited by chemical vapor deposition (CVD) with the reactant gas of $SiH_4$–$CH_4$–$NH_3$–$H_2$ mixture, hydrogen was inevitably introduced into film. For the SiCN:H films, Jedrzejowski et al. [15] reported the hardness values of the SiCN:H films higher than 27 GPa, while Awad et al. [17] reported that the hardness of the a-SiCN:H film varied in the range of 13–17 GPa and decreased with the increase of the N content. In comparison to the above-mentioned CVD methods, the SiCN films grown by PVD and ion implantation could avoid the poisonous gases such as $SiH_4$, $NH_3$ and $CH_4$. Lo et al. [1] reported that the hardness of the SiCN film synthesized by ion beam sputtering was 27–30 GPa. When the SiCN films were deposited on Si(1 0 0) substrates by dc magnetron co-sputtering of silicon and carbon using a single sputter target with variable Si/C area ratios in nitrogen–argon mixtures, the film hardness increased up to 40 GPa with the argon concentration in the gas mixture increasing from 0% to 75% [20]. If the SiCN films were deposited by arc enhanced magnetic sputtering hybrid system using a silicon target and graphite target in mixed gases of Ar

* Corresponding author. Tel.: +86 25 84893083; fax: +86 25 84893083.
*E-mail addresses:* fzhou@nuaa.edu.cn, zhoufei88cn@yahoo.com.cn (F. Zhou).

0925-8388/$ – see front matter © 2009 Elsevier B.V. All rights reserved.
doi:10.1016/j.jallcom.2009.11.063

and $N_2$, the maximum hardness of 35 GPa was acquired as the silicon content was 38 at.% [3]. If the SiCN films were deposited on Si(1 0 0), glass and stainless steel substrates by RF magnetron sputtering with assistant RF plasma, the hardness values of the SiCN films prepared with assistant RF plasma were higher than those without it [19], the formation of β-$C_3N_4$ crystallites was occurred in the amorphous matrix of the SiCN films, and the thermal mismatch between the substrate and the coating resulted in variation in deposition rate, roughness and other mechanical properties like hardness and adhesion for the three different substrates [21]. When the substrate temperature was lower or higher than 700 °C, the SiCN film had a loose structure with typical amorphous surface feature or was compactly covered with some spherical grains with diameter of about 50 nm [22]. The tribological properties of the SiCN films were related to their microstructure and composition, the low friction coefficient and low wear rate were acquired for the SiCN films with high carbon content [4–6]. The above reviews indicate that the physic-chemical properties of the SiCN films are strong functions of the process parameters.

As compared with the magnetron sputtering depositions, the dual ion beam sputtering (DIBS) has more available sputtering and deposition parameters owing to the adjustable location of ion sources, substrate and target. The synthesis mode of DIBS is that, the main source emits $Ar^+$ beam for target sputtering and the assisting source generates $N^+$ and $Ar^+$ beams, which synthesize the film on the substrate. By proper adjustment of dual ion beam parameters, this method permits a precise control of film composition, which is almost independent of deposition rate. Although the SiCN films have already been deposited using ion beam sputtering deposition (IBSD) [1,11,18], the researches related to the SiCN films deposited by DIBS are still limited. Therefore, the aim of this study is to investigate the influences of assisting ion energy and concentration on surface roughness, mechanical properties and bonding structure of the SiCN films deposited by sputtering of a SiC target with Ar–$N_2$ ion beam assistance using DIBS.

## 2. Experimental procedures

### 2.1. Deposition method of SiCN films

As seen in Fig. 1, the DIBS system has two Kaufman source ion guns (assist source ion gun I and main source ion gun II). The chamber was first evacuated to a background pressure of $5 \times 10^{-4}$ Pa with a turbo-molecular pump. Si(1 1 0) wafers, quartz substrate and NaCl single crystal substrates were mounted on a substrate holder with diameter of 10 cm. The substrate heater was turned on to keep the substrate temperature of 100 °C. In order to ensure the SiCN films with uniform thickness, the substrate holder was rotated at a speed of 1 rpm.

Before deposition, the surfaces for substrates and target were bombarded using $N^+$ and $Ar^+$ for 5 and 30 min, respectively. Then the SiCN films were deposited on Si(1 1 0) wafers, quartz substrate and NaCl single crystal using DIBS with a base pressure of $3.2 \times 10^{-2}$ Pa. During deposition, the main source ion gun II was first powered to generate $Ar^+$ ion beam at 800 eV and 50 mA, and then a high purity SiC target was sputtered by $Ar^+$ ions at an incidence angle of 45° from the target normal, while the assisting source ion gun I was powered to generate the mixture ion beam of $Ar^+$ and $N^+$ ions to bombard the film during its growth at an incidence of 60° from the sample normal. The assisting nitrogen ion beam concentration ($f_N$) varied in the range of 0.25–1 via adjusting the flow rates of Ar and $N_2$ gas. To obtain the SiCN films with different composition, the assisting source current was kept at 12 mA, while the assisting source ion beam energy ($E_a$) varied in the range of 100–300 eV. The deposition time was adjusted in the range of 1.5–2 h to obtain the SiCN films' thickness of 350 nm. The deposition parameters were listed in Table 1 in detail. The film thickness was measured using Micro XAM™ non-contact surface profilometer (ADE Phase-Shift, USA) on Si(1 1 0) wafer.

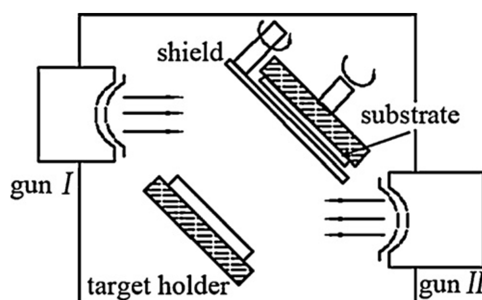


**Fig. 1.** Schematic diagram of dual ion beam sputtering (DIBS) chamber.

**Table 1**
Deposition parameters of the SiCN films.

| Parameter | Value |
|---|---|
| **Main source** | |
| Ion beam energy | 800 eV |
| Ion beam current | 50 mA |
| Ion beam composition | Ar |
| Cleaning time (targets) | 30 min |
| **Assisting source** | |
| Ion beam energy | 100–300 eV |
| Ion beam current | 12 mA |
| Ion beam composition | 0.25, 0.5, 0.75, 1.0 |
| Cleaning time (substrate) | 5 min |
| Chamber pressure | |
| Background | $5.0 \times 10^{-4}$ Pa |
| Operating | $3.2 \times 10^{-2}$ Pa |
| Substrates | Si(1 1 0), quartz and NaCl signal crystal |
| Films thickness | ≈350 nm |
| Rotating speed of substrate | 1 rpm |

### 2.2. Surface roughness and mechanical properties of SiCN films

The surface roughness of the SiCN films was measured by using Micro XAM™ non-contact surface profilometer. The hardness and elastic modulus of the SiCN films were evaluated by nano-indenter (MTS SA2, USA) with a Berkovich diamond. Load–unload curves were performed at a maximum load of 10 mN, and the maximum indentation depth was 120 nm. To obtain the error bars of the surface roughness, hardness and elastic modulus, three samples coated with the SiCN films

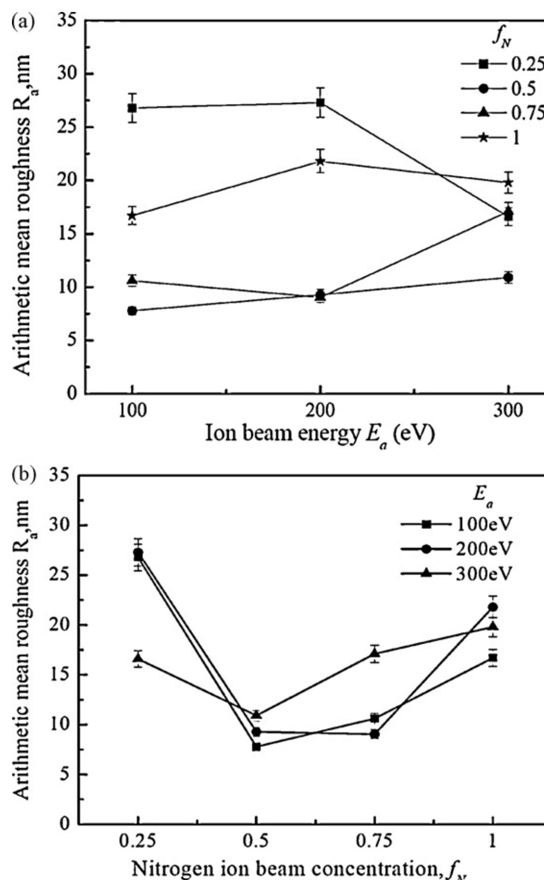


**Fig. 2.** Variation of the arithmetic mean roughness $R_a$ with the assisting ion beam energy (a) and concentration (b).

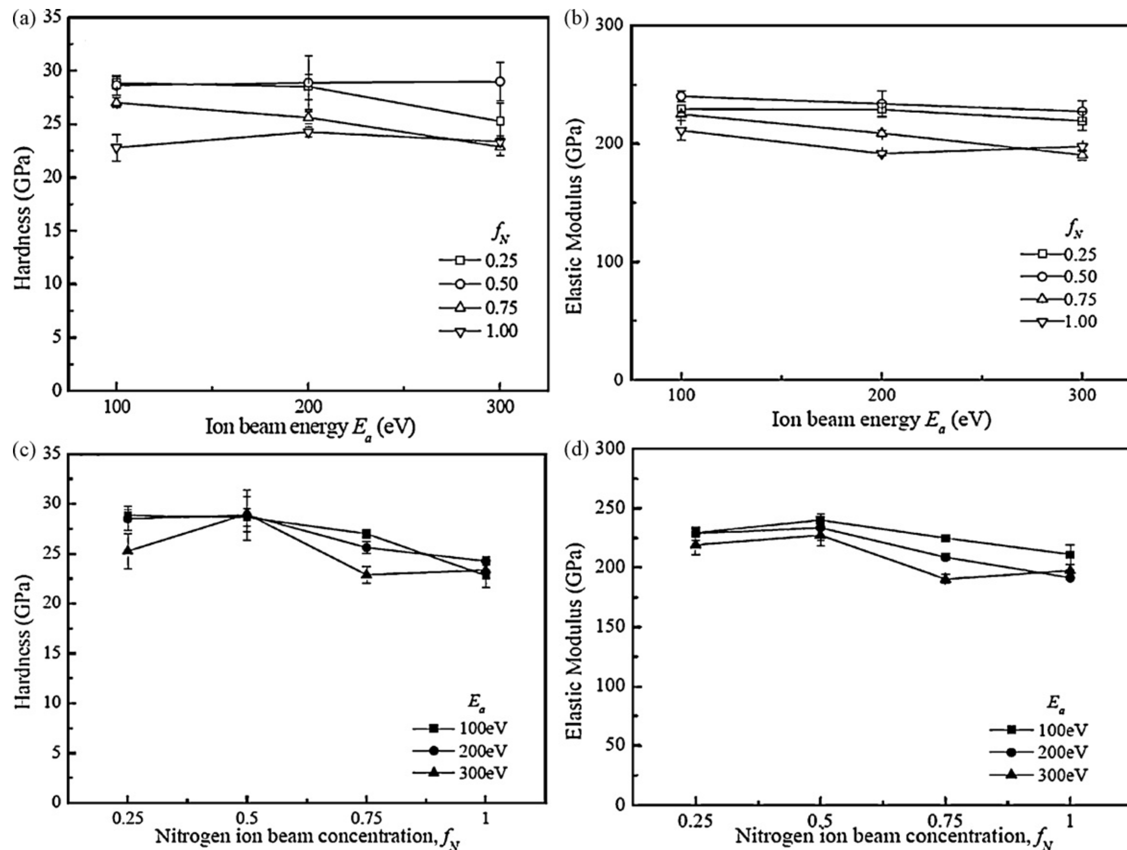


**Fig. 3.** Variation of hardness and elastic modulus with assisting ion beam energy (a and b) and concentration (c and d).

were first prepared under the same process condition. To ensure the accurate results, at least five measurement tests for surface roughness and ten measurement tests for hardness at different positions were carried out for one sample. The average results (surface roughness, hardness and elastic modulus) were obtained on the three samples under identical conditions.

*2.3. Chemical bonding structure of SiCN films*

The bonding structure of the SiCN films was analyzed using FT/IR-670 Fourier transform infrared spectra (JASCO, Japan) in the range of 500–4000 $cm^{-1}$ with a resolution of 1 $cm^{-1}$. The Raman spectra were obtained in the backscattering configuration between 250 and 2000 $cm^{-1}$ by JY-HR800 (J.Y. Company, France) using an argon ion laser at a wave number of 514 nm. Additionally, the chemical concentration and bonding structure of the SiCN films were determined using Thermo ESCALAB 250 X-ray photoelectron spectroscopy (XPS) with a 150 W $AlK_\alpha$ ($E$ = 1486.6 eV) X-ray source with beam diameter of 500 μm. The spectra of Si2p, C 1s, N 1s and O 1s were recorded at pass energies of 20 eV with a step size of 0.1 eV.

## 3. Results and discussion

### *3.1. Influence of assisting ion beam energy and concentration on surface roughness and mechanical properties of SiCN films*

The variation of surface roughness ($R_a$) with the assisting ion beam energy and concentration is shown in Fig. 2. When the assisting ion beam energy increased, the values of $R_a$ for the SiCN films deposited at the nitrogen ion beam concentration of 0.25 or 1.0 fluctuated in the range of 17–27 nm, while those at 0.75 first decreased to 9 nm at 200 eV, and then increased gradually. If the nitrogen ion beam concentration was 0.5, $R_a$ value slightly increased from 7 to 11 nm with increasing the assisting ion beam energy. It is clear from Fig. 2(b) that the surface roughness ($R_a$) first decreased to a minimum value at 0.5, and then increased gradually with an increase in the assisting ion beam concentration. Thus, the lowest surface roughness of 8 nm was obtained as the SiCN film deposited at the assisting ion beam energy of 100 eV and ion beam concentration of 0.5.

Fig. 3 shows the variations of hardness ($H$) and elastic modulus ($E$) of the SiCN films with the assisting ion beam energy and concentration. As seen in Fig. 3(a and b), the SiCN films deposited at the nitrogen ion beam concentration of 0.5 exhibited the high hardness and elastic modulus, which fluctuated slightly in the range of 28.6–29.0 and 240.2–227.3 GPa, respectively. Whereas the hardness and elastic modulus for the SiCN films deposited at the nitrogen ion beam concentration of 0.25 or 0.75 decreased gradually with the increase of the assisting ion beam energy. When the ion beam concentration was 1.00, the value of $H$ first increased to a peak value, and then decreased, but the variation tendency of $E$ was opposite to that of $H$. When the assisting ion beam concentration increased, as seen in Fig. 3(c and d), the hardness values for the SiCN films deposited at the assisting source ion energy lower than 300 eV decreased gradually, but the elastic modulus first increased to the peak value at 0.5, and then decreased. For the SiCN films at 300 eV, their hardness and elastic modulus zigzagged with the ion beam concentration. It is evident from Fig. 3 that the highest hardness of 29 GPa was obtained as the SiCN films were synthesized at the ion beam energy of 300 eV and the ion beam concentration of 0.5.

In order to know the relationship between surface roughness and the mechanical properties for the SiCN films, Figs. 2 and 3 were rearranged and illustrated as Fig. 4. It is obvious that the hardness and elastic modulus all first decreased as the surface roughness increased. When the film surface roughness was 17 nm, its hardness and elastic modulus all approached to the low values. Generally, the growth of the SiCN films is influenced [23] by (1) Re-sputtering of the deposited material as a result of the ion bombardment; (2) densification of the deposited materials by creation of energetic

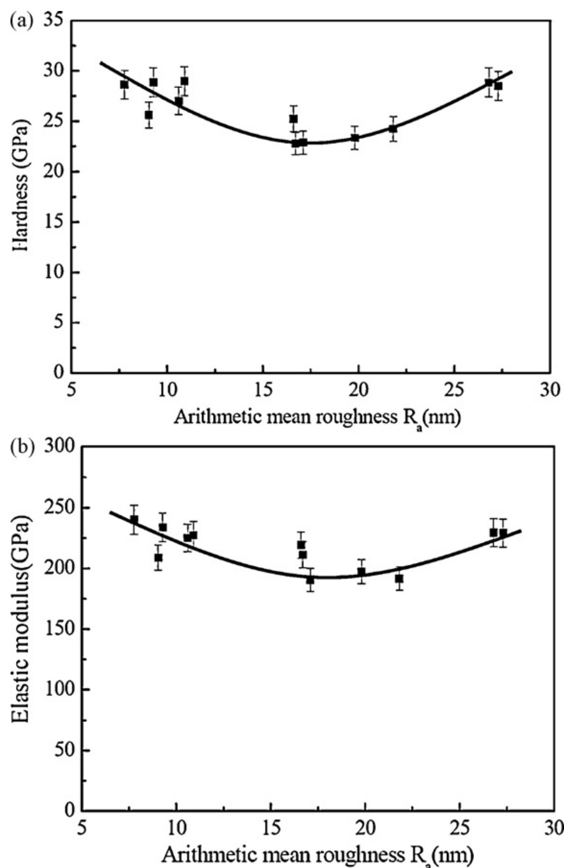


**Fig. 4.** Influence of surface roughness $R_a$ on hardness (a) and elastic modulus (b) for SiCN films.

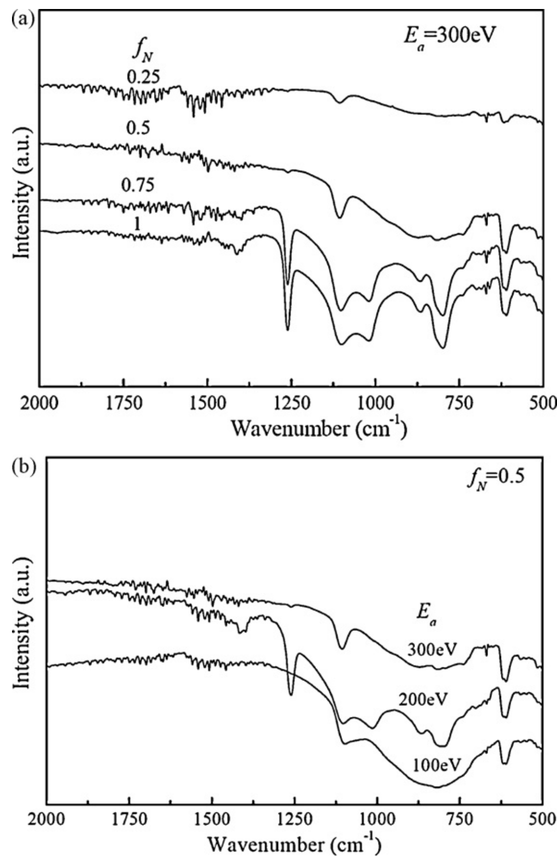


**Fig. 5.** FTIR spectra of the SiCN films grown on NaCl substrates at different ion composition with the fixed energy of 300 eV (a) and at different assisting ion beam energies for the fixed ion beam concentration of 0.5 (b).

bonding configurations; (3) incorporation of the incoming ions to the film as a solid product; (4) reaction ratio among nitrogen, silicon and carbon ions; (5) energy of nitrogen ion. Moreover, the results from Table 1 in Ref. [18] showed that the growth rate of the SiCN films increased with increasing sputtering voltage, and the silicon content of the SiCN films decreased at higher sputtering voltages. This indicated that the growth rate of the SiCN films decreased as the silicon content increased. In fact, the mechanical properties of the SiCN films were related not only to the composition and chemical bonding [1], but also to the denseness of the films [24]. As seen in Fig. 4, the SiCN films with the low or high surface roughness possessed the high hardness and elastic modulus. This indicated that the growth of SiCN coatings was influenced by the densification or sputtering caused by the energetic nitrogen ions bombardment, which had many influences on the mechanical properties of the SiCN films.

## *3.2. Influence of assisting ion beam energy and concentration on bonding structure of SiCN films*

### *3.2.1. Bonding structure analysis by FTIR spectroscopy*

As is known, FTIR spectrum serves as an indication of the bond vibration in thin films. Fig. 5(a) shows the influence of the assisting ion beam concentration on FTIR spectra of the SiCN films deposited at the assisting ion beam energy of 300 eV. When the assisting ion beam concentration increased, the broad band in 500–1000 $cm^{-1}$ displayed the obvious bonding structures. As the nitrogen ion beam concentration was 0.25, there were three stretching modes at 612, 673 and 790 $cm^{-1}$ between 500 and 1000 $cm^{-1}$. Refs. [25–27] reported the Si–C stretching modes corresponding to wavenumbers of 610, 655–677, 730–800, 818 and 877 $cm^{-1}$. This indicated that the stretching modes at 612, 673 and 790 $cm^{-1}$ between 500 and 1000 $cm^{-1}$ were assigned to the Si–C stretching mode. With an increase in wavenumber, there was one stretching mode at 1108 $cm^{-1}$ between 1000 and 1200 $cm^{-1}$, which was corresponded to Si–N stretching mode due to silicon nitride complex [25]. In the region between 1200 and 1800 $cm^{-1}$, there were three stretching modes at 1509, 1544 and 1714 $cm^{-1}$. Ref. [28] indicated that the broad bands in the range of 1200–1800 $cm^{-1}$ were representative of the C═N and C–N stretching modes. Ferrari et al. [29] pointed out that the C═C or C═N stretching modes were in the range of 1300–1600 $cm^{-1}$, but Sundaram and Alizdeh [25] reported that the C═C stretching mode was situated at 1456 $cm^{-1}$. So the absorption peaks at 1509, 1544 and 1714 $cm^{-1}$ could be assigned to the C═N stretching modes. When the assisting ion beam concentration was higher than 0.5, four stretching modes at 612, 673, 816 and 873 $cm^{-1}$ were observed and corresponded to the Si–C stretching mode. In the range of 1000–1200 $cm^{-1}$, two absorption peaks at 1021 and 1108 $cm^{-1}$ were corresponded to Si–O and Si–N stretching modes, respectively. In the range of 1200–1800 $cm^{-1}$, the peaks at 1261 and 1442 $cm^{-1}$ could be attributed to the C–N and C═C stretching modes, respectively, while the absorption peaks in the range of 1500–1800 $cm^{-1}$ could be assigned to the C═N stretching modes. As seen in Fig. 5(b), the FTIR spectra all displayed the Si–N stretching mode at 1104 $cm^{-1}$. When the assisting ion beam energy was 100 eV, two peaks in the range of 500–1000 $cm^{-1}$ were assigned to the Si–C stretching modes. As the wavenumber varied from 1200 to 1800 $cm^{-1}$, two peaks at 1457 and 1509 $cm^{-1}$ were assigned to the C═C and C═N stretching modes, respectively. If the assisting ion beam energy was higher than 100 eV, four peaks in the range of 500–1000 $cm^{-1}$ were attributed to the Si–C stretching modes. The band at 1021 $cm^{-1}$ was corresponded to Si–O stretching

**Table 2**
Influence of ion beam concentration on wavenumber of stretching modes of SiCN films.

| $f_N$ | Wave number of stretching modes ($cm^{-1}$) | | | | | |
|---|---|---|---|---|---|---|
| | Si–C | Si–O | Si–N | C–N | C=C | C=N |
| 0.25 | 612, 673, 790 | – | 1108 | – | | 1509, 1544, 1714 |
| 0.50 | 612, 673, 816, 873 | 1021 | 1108 | 1261 | 1442 | 1553, 1675 |
| 0.75 | 610, 673, 804, 864, | 1021 | 1104 | 1260 | 1400 | 1544, 1732 |
| 1.00 | 612, 673, 799, 869 | 1021 | 1104 | 1260 | 1413 | 1526, 1718 |

**Table 3**
Influence of ion beam energy on wavenumber of stretching modes of SiCN films.

| Ion beam energy (eV) | Wave number of stretching modes ($cm^{-1}$) | | | | | |
|---|---|---|---|---|---|---|
| | Si–C | Si–O | Si–N | C–N | C=C | C=N |
| 100 | 612, 816 | | 1100 | – | 1457 | 1509 |
| 200 | 612, 702, 803, 869 | 1017 | 1104 | 1260 | 1409 | 1509, 1540, |
| 300 | 612, 673, 816, 873 | 1021 | 1108 | 1261 | 1442 | 1500, 1553, 1675 |

mode [25]. In the range of 1200–1700 $cm^{-1}$, the peak at 1260 and 1409 $cm^{-1}$ could be attributed to the C–N and C=C stretching modes, while the absorption peaks at 1500–1800 $cm^{-1}$ could be assigned to the C=N stretching modes. It was clear that the bonding structures of the SiCN films changed from Si–C, Si–N, C=N bonds to Si–C, Si–O, Si–N, C=C, C–N, C=N bonds when the assisting ion beam concentration and energy increased. To know the stretching modes clearly, the wavenumber of stretching modes for the SiCN films deposited at different parameters were tabulated in Tables 2 and 3.

### 3.2.2. *Bonding structure analysis by Raman spectroscopy*

Raman spectra can give valuable information about the organization of carbon phases. The Raman spectra (Fig. 6) show only very broad bands due to the amorphous nature of the SiCN films and the peak Raman shift increases with the assisting ion beam concentration. As seen in Fig. 6(a), for the Raman spectrum of the SiCN films deposited at 100 eV, the mode at 926 $cm^{-1}$ in the region of 700–1200 $cm^{-1}$ was attributed to Si–N asymmetric stretching [13]. If the assisting ion beam energy was higher than 100 eV, the mode at 943 $cm^{-1}$ could be assigned to Si–N asymmetric stretching. The Raman shift in the region of 1200–1800 $cm^{-1}$ was assigned for carbon and its bonding attachment with silicon and nitrogen [13]. As seen in Fig. 6(b), in the region of 700–1200 $cm^{-1}$, the Raman spectrum at the assisting ion beam concentration of 0.25 showed no peak, while those at 0.5, 0.75 and 1.00 displayed the weak peaks. These weak peaks were situated at 943 $cm^{-1}$ for 0.5, 966 $cm^{-1}$ for 0.75 and 990 $cm^{-1}$ for 1.00, respectively. This indicated that the vibration mode changed from the Si–N asymmetric stretching to the SiC–N stretching [30] with an increase in the assisting ion beam concentration. But in the region of 1200–1800 $cm^{-1}$, the Raman bands were situated at 1410 $cm^{-1}$ for 0.25, 1444 $cm^{-1}$ for 0.5, 1450 for 0.75 and 1466 $cm^{-1}$ for 1.00, respectively. ∼1440 $cm^{-1}$ signature could be assigned to C–C bonds and its bonding attachment with silicon and nitrogen [29]. Ref. [31] reported that the Raman spectrum of $SiC_{1.18}$ exhibited a broadband centered at 1420 $cm^{-1}$ and was similar to that of $SiC_{0.6}N_{0.35}$ films at 1470 $cm^{-1}$. This C–C signature in Si–C alloys was described like a random covalent network of tetrahedral–trigonal bonding carbons (mixed $sp^2$–$sp^3$ hybridized bonds) with distorted bond angles and bond lengths. Although the amorphous SiCN films were more complicated due to their disordered structure and the presence of nitrogen, the network of tetrahedral–trigonal bonding carbons ($sp^2/sp^3$ hybridized bonds) should be linked with not only contain $Si(C_4)$ and $Si(N_4)$ units but also with mixed $Si(C_{4-n}N_n)$ tetrahedral. Thus, the Si–C, C–N, C=C and C=N bonds would exist in the mixed SiCN units and the $sp^2/sp^3$ hybridized binding the $Si(C_{4-n}N_n)$ tetrahedral.

In order to determine the precise band parameter in the range of 1200–1800 $cm^{-1}$, the Raman spectra of the SiCN films were fitted using Gaussians line shape. Fig. 7 shows the Raman spectrum of SiCN films at 0.5 and 300 eV and its deconvoluted peaks. After deducting background, all Raman spectra of the SiCN films could be deconvoluted into two peaks, and their Raman deconvoluted data were listed in Table 4. It is well known that the higher frequency band (∼1560 $cm^{-1}$) and the lower frequency band (∼1360 $cm^{-1}$) are generally recognized as G and D band for carbon films [32]. For the SiCN films, the band at 1560 $cm^{-1}$ could be assigned to the $sp^2$-coordinated C=N vibration and $sp^2$-hybridized C=C vibration whereas the 1360 $cm^{-1}$ band arose from limitation in the graphite

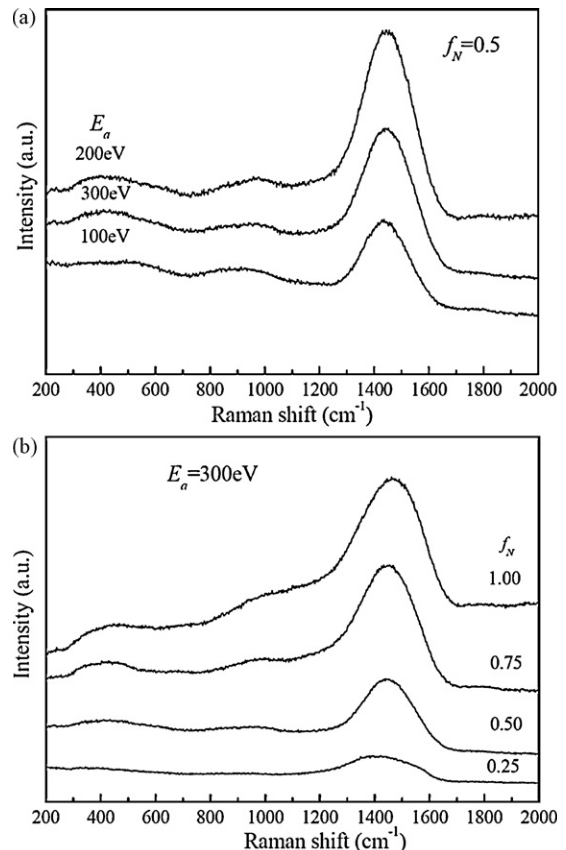


**Fig. 6.** Raman spectra of the SiCN films grown on quartz substrate at different ion energies with the fixed ion beam concentration of 0.5 (a) and at different assisting ion beam concentration for the fixed energy of 300 eV (b).

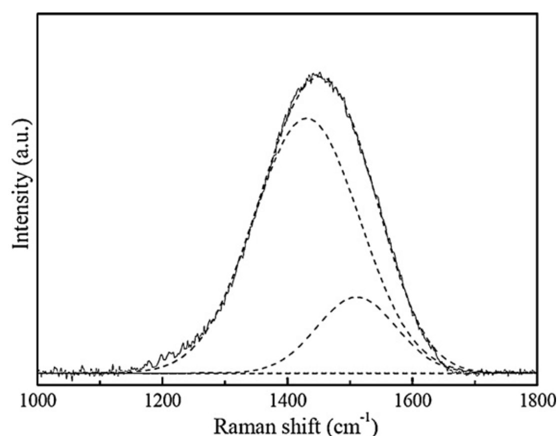


**Fig. 7.** Raman spectra of the SiCN films and deconvoluted peaks at the ion beam concentration of 0.5 and the ion beam energy of 300 eV.

domain size, induced by grain boundaries or imperfections, such as substitution N atoms, $sp^3$-coordinated carbons and nitrogen-bound $sp^3$-coordinated carbons[32]. As seen in Table 4, the deconvoluted peaks for the Raman spectra of the SiCN films were situated at 1428 and 1524 $cm^{-1}$ for 100 eV, 1431 and 1511 $cm^{-1}$ for 300 eV, while those at 200 eV were 1353 and 1457 $cm^{-1}$, respectively. Therefore, the peaks at 1428, 1431 and 1457 $cm^{-1}$ were attributed to the mixed $sp^2$–$sp^3$ hybridized bonds linked with not only contain $Si(C_4)$ and $Si(N_4)$ units but also with mixed $Si(C_{4-n}N_n)$ tetrahedral [31], while those at 1511 and 1524 $cm^{-1}$ were assigned to carbon attached to $O_2$ [28]. The peak at 1353 $cm^{-1}$ arose from nitrogen-bound $sp^3$-coordinated carbons. This indicates that the bonding structure for SiCN films at 100 and 300 eV mainly consists of the mixed $sp^2$–$sp^3$ hybridized bonds with $Si(C_4)$, $Si(N_4)$ and mixed $Si(C_{4-n}N_n)$ tetrahedral units, while the SiCN films at 200 eV consists of C–N bonds besides the mixed $sp^2$–$sp^3$ hybridized bonds with $Si(C_4)$, $Si(N_4)$ and mixed $Si(C_{4-n}N_n)$ tetrahedral units. It is obvious from Table 4 that the assisting ion beam concentration has more influences on the bonding structure of the SiCN films. When the assisting ion beam concentration increased, the Raman shift for the deconvoluted peaks decreased. The deconvoluted peaks were situated at 1402 and 1536 $cm^{-1}$ at 0.25; 1431 and 1511 $cm^{-1}$ at 0.50; 1344 and 1468 $cm^{-1}$ at 0.75, and 1353 and 1489 $cm^{-1}$ at 1.0, respectively. As above-mentioned, the deconvoluted peaks at 1344 and 1353 $cm^{-1}$ were attributed to nitrogen-bound $sp^3$-coordinated carbons, and those at 1431, 1468 and 1489 $cm^{-1}$ were assigned to the mixed $sp^2$–$sp^3$ hybridized bonds with $Si(C_4)$, $Si(N_4)$ and mixed $Si(C_{4-n}N_n)$ tetrahedral units. The deconvoluted peaks at 1511 and 1536 $cm^{-1}$ are due to carbon attached to $O_2$. The peak at 1402 $cm^{-1}$ was corresponded to the disordered $sp^2$ C, named the D′ peak [30]. This indicated that the SiCN films had the similar bonding structure at the assisting ion beam concentration higher than 0.5. As compared the analysis results of FTIR spectra with those of Raman spectra, it was concluded that the bonding structure of the SiCN films consisted of Si–C, Si–N, C–N, C=C and C=N bonds, which could exist as the mixed $sp^2$–$sp^3$ hybridized bonds with $Si(C_4)$, $Si(N_4)$ and mixed $Si(C_{4-n}N_n)$ tetrahedral units.

**Table 4**
Raman deconvoluted data for SiCN films.

| $E_a$ (eV) | $f_N$ | Raman shift ($cm^{-1}$) | Raman shift ($cm^{-1}$) |
|---|---|---|---|
| 100 | 0.50 | 1428 | 1524 |
| 200 | 0.50 | 1353 | 1457 |
| 300 | 0.25 | 1402 | 1536 |
| | 0.50 | 1431 | 1511 |
| | 0.75 | 1344 | 1468 |
| | 1.00 | 1353 | 1489 |

*3.2.3. Bonding structure analysis by XPS*

As seen in Figs. 2 and 3, the SiCN films deposited at 300 eV and 0.5 exhibited the excellent mechanical properties, and their concentration and chemical bonding were analyzed using XPS analysis. Fig. 8 shows the deconvoluted peaks of the corresponding chemical binding state of Si 2p, C 1s, N 1s and O 1s. As seen in Fig. 8(a), three peaks centered at 101.6, 102.6 and 103.3 eV were observed. Ref. [27] pointed out that the peaks centered at 101.8 and 102.5 eV were attributed to Si–C and Si–N bonds, respectively, and Ref. [20] reported that the Si–O bond was situated at the binding energy of 103.6 eV. This indicated that three peaks centered at 101.6, 102.6 and 103.3 eV were assigned to Si–C, Si–N and Si–O bonds, respectively. The curve fit of the C 1s spectrum (Fig. 8(b)) shows five peaks centered at 284.1, 284.6, 285.6, 286.3 and 287.7 eV. The peaks centered at 284.1 and 284.6 eV were assigned to Si–C and C=C bonds [9], while the peaks at 285.6 and 286.3 eV were corresponded to $sp^2$ C=N and $sp^3$ C–N bonds [33], respectively. The contribution of 287.7 eV revealed that carbon atom was bonded to oxygen as C–O [33]. When the SiCN films were deposited at a temperature below 100 °C from an adenine–silicon-mixture target sputtering by Ar ion beam [11,12], the Si–Si, Si–N, C–C, C=N and C–N bonds were observed. If the SiCN films were prepared from SiC/Si/C laminated target sputtering by nitrogen ion beam [1], the Si–N, C=N, C–N, C–O and Si–O bonds were found. This indicated that the Si–C bond was formed by using DIBS, but not formed by ion beam sputtering. For the curve fit of N 1s spectrum in Fig. 8(c), the peak at 398.9 eV was due to N–Si bond [9]. The peaks at 399.9 and 401.3 eV were assigned to $sp^3$ C–N and $sp^2$ C=N bonds [33]. For an O 1s core level line in Fig. 8(d), the binding energy of 533.35 eV was due to Si–O bond in the SiCN films [20]. This indicated that the chemical bonds in the SiCN films were Si–C, Si–N, C–N, C=N, C=C and Si–O bonds. The results were identical to the analysis of FTIR spectroscopy. If estimated in terms of peak area and atomic sensitivity factors, the ratio of C Si, N and O in the films expressed by the atomic ratios, C:Si:N:O was about 1:0.42:0.18:0.32.

*3.3. Discussion*

As seen in Figs. 2 and 3, when the assisting ion beam energy increased, the hardness of the SiCN films deposited at the ion beam concentration of 0.5 increased from 28.6 to 29 GPa, while the elastic modulus decreased. If the SiCN films were deposited at the ion beam energy of 300 eV, the values of $H$ and $E$ first increased to the maximum values at the ion beam concentration of 0.5, and then decreased with the increase of the assisting ion beam concentration. Actually, the mechanical properties of the SiCN films were governed by the formation of bonding structure and the denseness of the film. The formation of bonding structure was related to the reaction among sputtered Si, C atoms and nitrogen ions, whereas the denseness of the film was influenced by the growth rate. Wu and co-workers [12] reported that the growth rate of the SiCN films increased with increasing sputtering voltage while decreased with increasing the silicon content. With an increase in the $N_2$/Ar flow rate, the deposition rate and the surface roughness of the SiCN films decreased [24,25]. Vlček et al. [20] reported that the sputtering of carbon was strongly chemically driven by reactions between carbon and nitrogen, while the sputtering of silicon was more effective than that of carbon in the discharges with high argon content. With rising argon concentration in the gas mixture, the Si content in the SiCN films increased while the C content decreased, which led to higher hardness of the SiCN films [20]. Awad et al. [17] reported that the increase incorporation of N

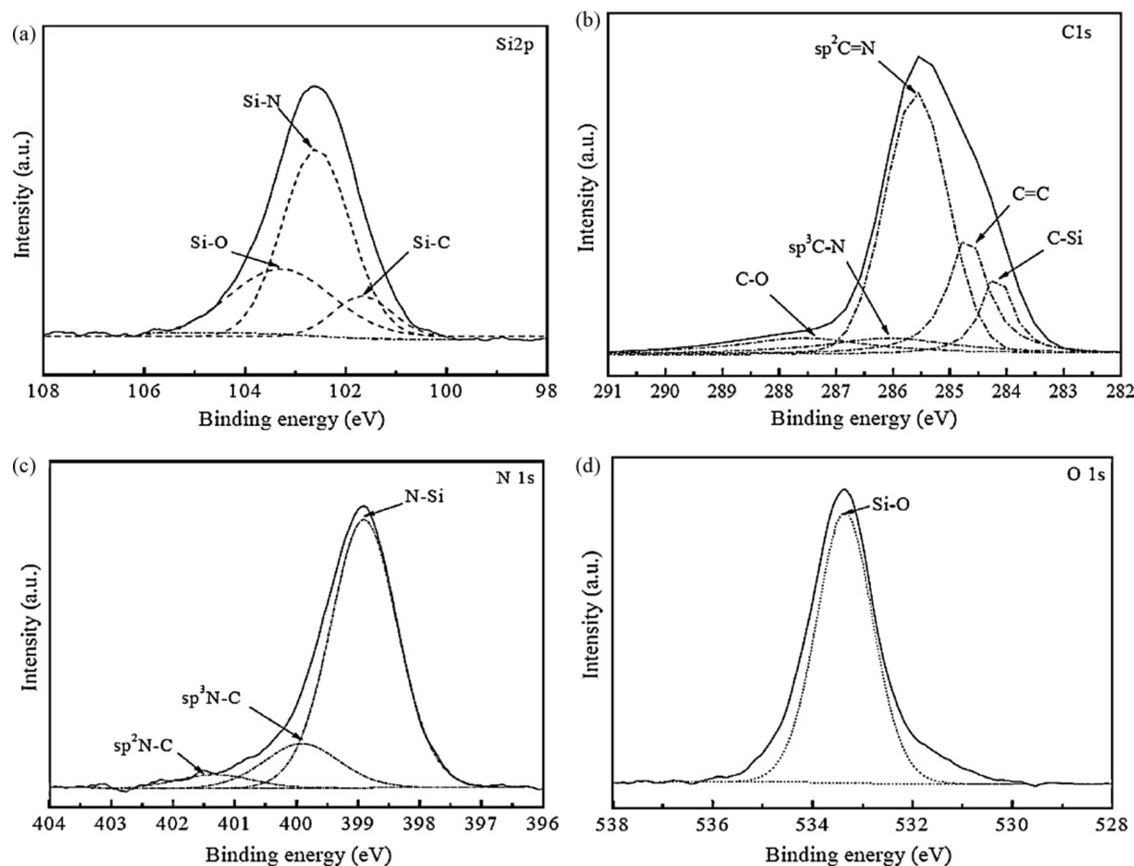


**Fig. 8.** X-ray photoelectron spectra of SiCN film deposited at the ion beam energy of 300 eV and the nitrogen ion beam concentration of 0.5: (a) Si 2p, (b) C ls, (c) N ls, (d) O 1s.

in the a-SiCN:H films resulted in an increase of the average surface roughness from 4 to 12 nm, and both *H* and *E* of the a-SiCN:H films decrease from ~17 and 160 GPa to ~13 and 136 GPa, respectively when the N content is increased from 0% to 27 at.%. It was concluded that the assisting ion beam concentration was the major factor. When the assisting ion beam concentration was lower than 0.5, the *H* and *E* values were higher than 25 and 219 GPa, respectively. This indicated that the mechanical properties of the SiCN films were related to their chemical bonding structure. As seen in Tables 2 and 3, it was clear that the bonding structure of SiCN films at the assisting ion beam concentration lower than 0.5 consisted of Si–C, Si–N, C=C and C=N bonds. Furthermore, the XPS analysis showed low nitrogen concentration in the SiCN films. This revealed that the C-rich SiCN film was formed as the assisting ion beam concentration was lower than 0.5. In the case of C-rich SiCN films, the C–N bond was negligible while the proportion of Si–C bond was highest. Awad et al. [17] indicated that the hardness and elastic modulus of the SiCN:H films increased linearly with the Si–C bond density. Furthermore, Si–C bond provided a higher hardness than Si–N bond [31]. Thus, the C-rich SiCN films possessed the higher values of *H* and *E*. As the assisting ion beam concentration was higher than 0.5, N preferentially bonded to C and Si, and then the SiCN films became the N-rich SiCN films. Thus, the bonding structure of the SiCN films consisted of Si–C, Si–N, Si–O, C–N, C=C and C=N bonds (Table 2). For the N-rich SiCN films, Si bonded with C was substituted by N to form C–N and C=N bonds and on the other hand, C bonded with Si was substituted by N to give Si–N bonds. This indicated that the number of Si–N, C=N, C–N and C=C bonds increased, which caused the decrease of both *H* and *E*. Thus, the mechanical properties of the SiCN films were correlated to the proportion of Si–C, Si–N, C=N and C–N bonds in the SiCN films.

## 4. Conclusions

The influences of assisting ion beam energy and concentration on surface roughness, mechanical properties and bonding structure of the SiCN films have been studied. The main results could be summarized as:

1. When the assisting ion beam energy varied in the range of 100–300 eV, the surface roughness and the hardness of SiCN films fluctuated in the range 7–27 nm and 23–29 GPa, respectively.
2. With an increase in the ion beam concentration, the surface roughness of the SiCN films first decreased to a low value, and then increased, while the hardness first increased to a high value, and then decreased.
3. When the assisting nitrogen ion beam energy and concentration increased, the bonding structures of SiCN films changed from Si–C, Si–N, C=N bonds to Si–C, Si–O, Si–N, C=C, C–N, C=N bonds and showed the mixed $sp^2$–$sp^3$ hybridized bonds linked with $Si(C_4)$, $Si(N_4)$ and $Si(C_{4-n}N_n)$ tetrahedral units.
4. When the SiCN films were deposited at the ion beam energy of 300 eV and the ion beam concentration of 0.5, the low surface roughness of 11 nm and the high hardness of 29 GPa were obtained, and the atomic ratios, C:Si:N:O was about 1:0.42:0.18:0.32. The mechanical properties of the SiCN films were correlated to the proportion of Si–C, Si–N, C=N and C–N bonds in the SiCN films.

## Acknowledgement

The authors would like to express their appreciation to Xumin Yang and Yonghui Zhang for their helps in films' deposition and roughness measurement. This work is supported by the Nation Natural Science Foundation of China (no. 50675102) and the Natural Science Foundation of Jiangsu Province (no. BK2007529). We would like to acknowledge NNSFC and NSFJS for financial support.

## References

[1] H.C. Lo, J.J. Wu, C.Y. Wen, T.S. Wong, S.T. Lin, K.H. Chen, L.C. Chen, Diamond Relat. Mater. 10 (2001) 1916–1920.
[2] P. Gao, J. Xu, Y. Piao, W. Ding, D. Wang, X. Deng, C. Dong, Surf. Coat. Technol. 201 (2007) 5298–5301.
[3] S.L. Ma, B. Xu, G.Z. Wu, Y.F. Wang, F. Ma, D.Y. Ma, K.W. Xu, T. Bell, Surf. Coat. Technol. 202 (2008) 5379–5382.
[4] H. Hoche, D. Allebrandt, M. Bruns, R. Riedel, C. Fasel, Surf. Coat. Technol. 202 (2008) 5567–5571.
[5] F. Zhou, Y.G. Yuan, K.M. Chen, X.L. Wang, Nuclear Inst. Methods Phys. Res. B 267 (2009) 2858–2865.
[6] F Zhou, Y.G. Yuan, X.L. Wang, M.L. Wang, Appl. Surf. Sci. 255 (9) (2009) 5079–5087.
[7] T. Nakayamada, K. Matsuo, Y. Hayashi, A. Izumi, Y. Kadotani, Thin Solid Films 516 (2008) 656–658.
[8] D. Pech, N. Schupp, P. Steyer, T. Hack, Y. Gachon, C. Héau, A.S. Loir, J.C. Sánchez-López, Wear 266 (2009) 832–838.
[9] X.W. Du, Y. Fu, J. Sun, P. Yao, L. Cui, Mater. Chem. Phys. 103 (2007) 456–460.
[10] K. Kobayashi, H. Yokoyama, M. Endoh, Appl. Surf. Sci. 254 (2008) 6222–6225.
[11] L.C. Chen, C.T. Wu, J.J. Wu, K.H. Chen, Int. J. Mod. Phys. B 14 (2000) 333–348.
[12] C.W. Chen, C.C. Huang, Y.Y. Lin, L.C. Chen, K.H. Chen, Diamond Relat. Mater. 14 (2005) 1126–1130.
[13] B.P. Swain, N.M. Hwang, Appl. Surf. Sci. 254 (2008) 5319–5322.
[14] A. Limmanee, M. Otsubo, T. Sugiura, T. Sato, S. Miyajima, A. Yamada, M. Konagai, Thin Solid Films 516 (2008) 652–655.
[15] P. Jedrzejowski, J. Cizek, A. Amassian, J.E. Klemberg-Sapieha, J. Vlcek, L. Martinu, Thin Solid Films 447/448 (2004) 201–207.
[16] P. Kouakou, M. Belmahi, V. Brien, V. Hody, H. Migeon, J. Bougdira, Surf. Coat. Technol. 203 (2008) 277–283.
[17] Y. Awad, M.A. El Khakani, C. Aktik, J. Mouine, N. Camire, M. Lessard, M. Scarlete, H.A. Al-Abadleh, R. Smirani, Surf. Coat. Technol. 204 (2009) 539–545.
[18] J.J. Wu, C.T. Wu, Y.C. Liao, T.R. Lu, L.C. Chen, K.H. Chen, L.G. Hwa, C.T. Kuo, K.J. Ling, Thin Solid Films 355–356 (1999) 417–422.
[19] W.L. Li, J.L. Yang, Y. Zhao, W.D. Fei, J. Alloys Compd. 482 (2009) 317–319.
[20] J. Vlček, M. Kormunda, J. Čĺzek, Z. Soukup, V. Peřina, J. Zemek, Diamond Relat. Mater. 12 (2003) 1287–1294.
[21] A.S. Bhattacharyya, S.K. Mishra, S. Mukherjee, G.C. Das, J. Alloys Compd. 478 (1–2) (2009) 474–478.
[22] Z. Chen, H. Lin, J. Zhou, Z. Ma, E. Xie, J. Alloys Compd. 487 (1–2) (2009) 531–536.
[23] R. Gago, I. Jiménez, J.M. Albella, Thin Solid Film 373 (2000) 277–281.
[24] Z. Alizadeh, K.B. Sundaram, S. Seal, Appl. Surf. Sci. 183 (2001) 270–277.
[25] K.B. Sundaram, J. Alizdeh, Thin Solid Films 370 (2000) 151–154.
[26] X.C. Wu, R.Q. Cai, P.X. Yan, W.M. Liu, J. Tian, Appl. Surf. Sci. 185 (2002) 262–266.
[27] E. Xie, Z. Ma, H. Lin, Z. Zhang, D. He, Opt. Mater. 23 (2003) 151–156.
[28] M.R. Wixom, J. Am. Ceram. Soc. 73 (1990) 1973–1978.
[29] A.C. Ferrari, S.E. Rodil, J. Robertson, Phys. Rev. B 67 (2003), pp. 155306-1-1155306-20.
[30] Y.H. Cheng, B.K. Tay, S.P. Lau, X. Shi, X.L. Qiao, J.G. Chen, Y.P. Wu, C.S. Xie, Appl. Phys. A73 (2001) 341–345.
[31] A. Bendeddouche, R. Berjoan, E. Bêche, R. Hillel, Surf. Coat. Technol. 111 (1999) 184–190.
[32] E.J. Liang, J.W. Zhang, J. Leme, C. Moura, L. Cunha, Thin Solid Films 469–470 (2004) 410–415.
[33] F. Zhou, K. Adachi, K. Kato, Thin Solid Films 514 (2006) 231–239.